Spin-reversal energy barriers of 305 K
for Fe^{2+} d^6 ions with linear ligand coordination

Lei Xu,[1] Ziba Zangeneh,[1] Ravi Yadav,[1] Stanislav Avdoshenko,[2]
Jeroen van den Brink,[1,3] Anton Jesche,[4] and Liviu Hozoi[1]

[1]*Institute for Theoretical Solid State Physics, IFW Dresden, Helmholtzstr. 20, 01069 Dresden, Germany*
[2]*Institute for Solid State Research, IFW Dresden, Helmholtzstr. 20, 01069 Dresden, Germany*
[3]*Department of Physics, Technical University Dresden, Helmholtzstr. 10, 01069 Dresden, Germany*
[4]*Center for Electronic Correlations and Magnetism,*
Augsburg University, Universitätsstr. 1, 86135 Augsburg, Germany
(Dated: October 14, 2019)

A remarkably large magnetic anisotropy energy of 305 K is computed by quantum chemistry methods for divalent Fe^{2+} d^6 substitutes at Li-ion sites with D_{6h} point-group symmetry within the solid-state matrix of Li$_3$N. This is similar to values calculated by the same approach and confirmed experimentally for linearly coordinated monovalent Fe^{1+} d^7 species, among the largest so far in the research area of single-molecule magnets. Our *ab initio* results therefore mark a new exciting exploration path in the search for superior single-molecule magnets, rooted in the $d^{1.5}_{xy}d^{1.5}_{x^2-y^2}d^1_{z^2}d^1_{yz}d^1_{zx}$ configuration of d^6 transition-metal ions with linear or quasilinear nearest-neighbor coordination. This d^6 axial anisotropy may be kept robust even for symmetries lower than D_{6h}, provided the ligand and farther-neighbor environment is engineered such that the $d^{1.5}_{xy}d^{1.5}_{x^2-y^2}d^1_{z^2}d^1_{yz}d^1_{zx} - d^1_{xy}d^1_{x^2-y^2}d^2_{z^2}d^1_{yz}d^1_{zx}$ splitting remains large enough.

The notion of single-molecule magnet (SMM) came into the field of quantum magnetism with recognizing that certain molecules may display, as individual entities, the essential features of magnetic nanoparticles: large-spin electron configurations, strong axial anisotropy and a sizable energy barrier between the two stable orientations of the total magnetic moment such that, below a certain 'blocking' temperature, the system can be trapped in one of those two states. Below the blocking temperature SMM's exhibit therefore magnetic hysteresis. Such effects have only been observed at rather low temperatures so far but intensive work is going on to identify systems with superior properties in this regard: higher blocking temperatures, longer relaxation times and larger coercivity fields. An impelling idea is realizing regular, stable arrays of such molecules for high-density data storage [1], provided that the associated blocking temperatures and relaxation times are appropriately optimized.

SMM physics was first pointed out by Sessoli *et al.* for a Mn$_{12}$ complex, in 1993 [2]. Since then the field advanced dramatically, with dozens of new SMM's being reported, either d-metal or f-metal based. As concerns their specific magnetic properties, the most remarkable are nowadays the Tb^{3+} and Dy^{3+} SMM's with N$_2^{3-}$ ligand bridges [3, 4], some lanthanide single-ion magnets with high-symmetry environment [5], the fullerene-encapsulated f-electron SMM's [6] and the linear Fe^{1+} complexes [7]. Interestingly, SMM-like behaviour has been also identified recently for linearly coordinated Fe-ion substitutes within the solid-state matrix of Li$_3$N [8]. The latter findings [7, 8] open new research avenues in this field because, due to the well known 'orbital quenching' issue in transition-metal (TM) compounds, mononuclear d-metal

ions have been rarely considered as good candidates to achieving first rate SMM characteristics.

The electronic structure and magnetic anisotropy of Fe ions placed within the Li$_3$N lattice have been investigated on the theoretical side by calculations based on density functional theory (DFT) [9–12]. A Fe^{1+} d^7 valence electron configuration has been assumed in the DFT studies [10–12] but diffraction [13, 14] and x-ray absorption experiments on TM centers within the Li$_3$N matrix suggest 2+ valence states for d-metal ions in such an environment [15]. Here we provide unbiased *ab initio* results of many-body quantum chemistry calculations for both Fe^{1+} d^7 and Fe^{2+} d^6 species at a Li lattice site. The computed Fe^{1+} d^7 excitation spectrum indicates an axial magnetic anisotropy of 31 meV for linear N-Fe-N coordination, in agreement with experimental results for relatively large amount of Fe cation substitution [8, 16]. What is more, the calculated magnetic anisotropy reaches values of similar magnitude for Fe^{2+} d^6, 26.3 meV (i.e., 305 K), if the overall lattice symmetry is not broken by vacancies in the immediate neighborhood. This is related to an unexpected $d^1_{z^2}d^{1.5}_{xy}d^{1.5}_{x^2-y^2}d^1_{yz}d^1_{zx}$ ground-state configuration in which due to subtle many-body effects one electron is removed from the 'deeper' d_{z^2} level [10–12], as compared to the Fe^{1+} $d^2_{z^2}d^{1.5}_{xy}d^{1.5}_{x^2-y^2}d^1_{yz}d^1_{zx}$ ground state. With a vacant nearest-neighbor (NN) Li site — which ensures charge neutrality and coincides with a Li$_{3-2x}$TM$_x^{2+}$N picture [15] for the substitution process — the interaction between the $d^1_{z^2}d^{1.5}_{xy}d^{1.5}_{x^2-y^2}d^1_{yz}d^1_{zx}$ and $d^2_{z^2}d^1_{xy}d^1_{x^2-y^2}d^1_{yz}d^1_{zx}$ states, arising from breaking the symmetry around the Fe^{2+} ion, reduces the magnetic anisotropy to ≈15 meV. The latter number provides an explanation for the strong reduction of the magnetic

anisotropy observed experimentally in the very dilute system [16] and support for the $\text{Li}_{3-2x}\,\text{TM}^{2+}\text{N}$ model [15] at very small concentrations of TM centers. Corroborated with earlier experimental results [15, 16], our computational data can therefore reconcile the $\text{Li}_{3-x}\,\text{TM}_x^{1+}\text{N}$ and $\text{Li}_{3-2x}\,\text{TM}_x^{2+}\text{N}$ cation-substitution models, suggesting that due to finite concentration of Li-ion vacancies the TM 2+ valence state dominates in the very dilute TM:Li$_3$N system while TM 1+ plays a dominant role at large concentrations of TM species. Most importantly, our findings draw attention to the very large magnetic anisotropy associated with the Fe^{2+} $d_{z^2}^1 d_{xy}^{1.5} d_{x^2-y^2}^{1.5} d_{yz}^1 d_{zx}^1$ configuration in full D_{6h} symmetry, analogous to Fe^{1+} values defining so far the largest magnetic anisotropies in the SMM research area [7, 8].

Relative energies describing the excitation spectrum of the Fe^{1+} $3d^7$ center are provided in Table I. We focus on cation substitution at linearly coordinated 1b Li sites, since that is the geometrical configuration maximizing the single-ion magnetic anisotropy [7, 10]. The many-body quantum chemistry calculations were performed on $[\text{FeN}_2\text{Li}_{14}]^{9+}$ clusters as depicted in Fig. 1, embedded within a large array of point charges which reproduces the Madelung field of the Li$_3$N lattice. All-electron basis sets as described in Methods were employed for the $[\text{FeN}_2\text{Li}_{14}]$ unit. In a first step, the orbitals were optimized for an average of all d^7 high-spin ($S=3/2$) states using the multiconfigurational complete-active-space self-consistent-field (CASSCF) approach [17]. This ensures a balanced description of all d^7 electron configurations: $a_{1g}^2 e_{2g}^3 e_{1g}^2$, $a_{1g}^2 e_{2g}^2 e_{1g}^3$, $a_{1g}^1 e_{2g}^3 e_{1g}^3$, $a_{1g}^1 e_{2g}^4 e_{1g}^2$ and $a_{1g}^1 e_{2g}^2 e_{1g}^4$, where d_{z^2} belongs to the A_{1g} irreducible representation, $\{d_{xy}, d_{x^2-y^2}\}$ to E_{2g} and $\{d_{yz}, d_{zx}\}$ to E_{1g}, for D_{6h} point-group symmetry. Following the CASSCF calculation, multireference configuration-interaction (MRCI) computations with single and double excitations were performed [17, 18]. Spin-orbit couplings were subsequently accounted for according to the procedure described in Ref.[19]. We utilized the quantum chemistry package MOLPRO [20] and Li$_3$N lattice parameters as derived in Ref.[21]. Yet we allowed relaxation of the N-Fe-N bonds, i.e., for the two nitrogen ions adjacent to the Fe cation we determined the z-axis positions which minimize the total energy while fixing all other lattice coordinates as in the unmingled Li$_3$N crystal. At the MRCI level, the 'relaxed' Fe^{1+}-N bond lengths are 1.92 Å, slightly shorter than the experimental Li-N distances along the z axis [21].

In the described MRCI+SOC computational frame, we predict three main sets of excited states (see Table I): low-lying excited states related to the magnetic anisotropy of the ($S=3/2$, $L=2$) $a_{1g}^2 e_{2g}^3 e_{1g}^2$ configuration in the range of $\lesssim 100$ meV, high-spin e_{2g} to e_{1g} excitations at 1.1–1.2 eV and a multitude of crystal-field excitations from 1.75 eV onwards. The a and b labels in Table I are used in order to distinguish between states

TABLE I. $3d$-shell energy levels for a Fe^{1+} ion at the Li 1b crystallographic position in Li$_3$N; unless otherwise specified, units of eV are used. All $3d^7$ $S=3/2$ and the few lowest $S=1/2$ states are listed. The spin-orbit calculations provide three main groups of Kramers doublets: between 0 and 100 meV, at 1.1–1.2 eV and from 1.75 eV onwards.

Fe^{1+} $3d^7$ splittings	CASSCF	MRCI	MRCI+SOC
$^4E_{2g}$ $(a_{1g}^2 e_{2g}^3 e_{1g}^2)$	0	0	0, 30, 62, 96 meV
$^4E_{1g}$ $(a_{1g}^2 e_{2g}^2 e_{1g}^3)$	0.91	1.09	1.11 − 1.16
$a\,^4E_{1g}$ $(a_{1g}^1 e_{2g}^3 e_{1g}^3)$	1.50	1.78	1.75
$a\,^4A_{2g}$ $(a_{1g}^1 e_{2g}^4 e_{1g}^2,\, a_{1g}^1 e_{2g}^2 e_{1g}^4)$	1.67	1.87		
$a\,^2E_{2g}$ $(a_{1g}^2 e_{2g}^3 e_{1g}^2)$	2.23	2.05		
$^2E_{1g}$ $(a_{1g}^2 e_{2g}^4 e_{1g}^1)$	2.25	2.11		
$b\,^2E_{2g}$ $(a_{1g}^2 e_{2g}^3 e_{1g}^2)$	2.29	2.11		
$^2E_{1g}$ $(a_{1g}^2 e_{2g}^3 e_{1g}^2)$	2.50	2.35	2.41
$b\,^4E_{1g}$ $(a_{1g}^1 e_{2g}^2 e_{1g}^3)$	2.69	2.70	
$b\,^4A_{2g}$ $(a_{1g}^1 e_{2g}^4 e_{1g}^2,\, a_{1g}^1 e_{2g}^2 e_{1g}^4)$	3.27	3.28	

implying the same electron configuration, irreducible representation and spin multiplicity. The spin-orbit treatment was carried out in terms of all $S=3/2$ quartets and those doublets with MRCI relative energies of less than 2.5 eV. The lowest excited state, defining the magnetic anisotropy energy, lies in this case at 30 meV. If the orbitals are optimized just for the $a_{1g}^2 e_{2g}^3 e_{1g}^2$ ground-state configuration, this particular excitation energy changes to 31 meV.

Results of similar type are provided in Table II for the Fe^{2+} d^6 configuration. What makes this valence electron configuration worth investigating is the observation that a finite amount of vacant Li sites would necessarily require a higher ionized state for some of the TM centers, according to a $\text{Li}_{3-x-2y}\text{Fe}_x^{1+}\text{Fe}_y^{2+}\text{N}$ picture. The very surprising result for the Fe^{2+} d^6 ion is that the computed ground-state electron configuration defies a simple diagram of single-electron levels according to which, from the Fe^{1+} $a_{1g}^2 e_{2g}^3 e_{1g}^2$ 'reference', removal of one additional electron yields a $a_{1g}^2 e_{2g}^2 e_{1g}^2$ orbital occupation [11, 12]. Instead, the quantum chemistry calculations indicate the $3d$-shell Coulomb interactions are such that it is energetically more favorable to remove one electron from the apical a_{1g} d_{z^2} orbital rather than further depleting the 'in-plane' e_{2g}'s, d_{xy} and $d_{x^2-y^2}$. An important detail here is that there are no negatively charged ions in the plane within which the lobes of the latter lie while the former points to anions with formal 3− charges. Consequently, the $3d^6$ ground-state configuration is $a_{1g}^1 e_{2g}^3 e_{1g}^2$ according to our calculations, with an occupation of the e_g levels that provides again a large angular momentum ($L=2$) and strong axial anisotropy. Using orbitals optimized for an average of all $S=2$ d^6 states, the magnetic anisotropy energy comes as 26.3 meV in the d^6 spin-orbit MRCI calculation (see Table II); the same value, 26.3 meV, is obtained with orbitals optimized just for the lowest two
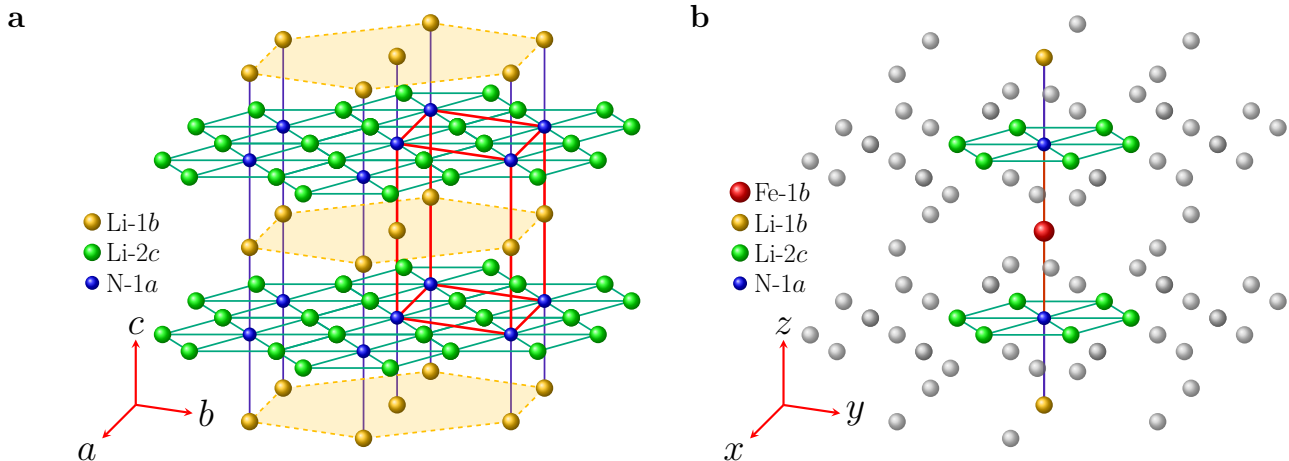
a

b

FIG. 1.   a) Crystal structure of Li_3N, with Li_2N honeycomb layers separated by Li-$1b$ sites. The crystallographic unit cell is indicated as a red polyhedron. b) Configuration of nearby sites around a Fe cation at the $1b$ crystallographic position in Li_3N. These sites define the fragment treated at the all-electron quantum mechanical level in our calculations. The extended solid-state surroundings are modeled as a large array of point charges, depicted here as small grey spheres. A similar type of linear coordination of the Fe ion (Fe^{1+} d^7) is found in certain molecular systems [7].

quintet states. That is 305 K, room-temperature energy scale.

Also for these computations, we considered all the high-spin ($S=2$) states in the spin-orbit treatment but only the spin triplets and singlets with MRCI relative energies of less than 2.8 eV. As for the Fe^{1+} d^7 ion, the different m_J states associated with the ground-state configuration cover an energy window extending up to ≈ 100 meV. The first crystal-field excitation, however, implies here an energy scale of only ≈ 200 meV; that is the $^5E_{2g}$ ($a^1_{1g}e^3_{2g}e^2_{1g}$) to $^5A_{1g}$ ($a^2_{1g}e^2_{2g}e^2_{1g}$) transition. Other excited states lie in the energy range of 1.2–1.3 eV and from 1.8 eV onwards. All these results correspond to 'relaxed' Fe^{2+}-N bonds of 1.88 Å. Significant shortening of the N-TM-N bonds has been also inferred from EXAFS measurements on TM ions embedded within the solid-state Li_3N matrix [15].

To retain overall charge neutrality, for the set of calculations whose results are summarized in Table II, we compensated the larger, 2+ valence state of the Fe ion by adding one (negative) electronic charge to the nearby crystalline surroundings. In particular, we equally distributed this elementary negative charge over the six closest Li $1b$ sites within the xy plane. This way, the D_{6h} point-group symmetry at the Fe site is preserved. An additional set of calculations was then performed with one of the NN Li ions at a $2c$ crystallographic position explicitly removed from the cluster described by quantum chemistry methods. This also preserves overall charge neutrality, according to the $Li_{3-2x}TM^{2+}_xN$ model of Muller-Bouvet *et al.* [15]. The symmetry being lower with such a Li vacant site, the $a^1_{1g}e^3_{2g}e^2_{1g}$ and $a^2_{1g}e^2_{2g}e^2_{1g}$ configurations, in particular, can interact and admix. As

TABLE II. $3d$-shell energy levels for a Fe^{2+} ion at the Li $1b$ crystallographic position in Li_3N; unless otherwise specified, units of eV are used. All $3d^6$ $S=2$ and the lowest $S=1$ and $S=0$ states are listed. The spin-orbit calculations provide four main groups of excited states: up to ≈ 105 meV, 180–200 meV, 1.2–1.3 eV and from 1.8 eV onwards.

Fe^{2+} $3d^6$ splittings	CASSCF	MRCI	MRCI+SOC
$^5E_{2g}$ ($a^1_{1g}e^3_{2g}e^2_{1g}$)	0	0	0, 26, 52, 78, 104 meV
$^5A_{1g}$ ($a^2_{1g}e^2_{2g}e^2_{1g}$)	0.26	0.14	0.18 – 0.19
$^5E_{1g}$ ($a^1_{1g}e^2_{2g}e^3_{1g}$)	1.09	1.18	1.21 – 1.26
$a\,^3E_{1g}$ ($a^1_{1g}e^3_{2g}e^1_{1g}$)	2.31	1.84	1.84
$b\,^3E_{1g}$ ($a^2_{1g}e^3_{2g}e^1_{1g}$)	2.37	1.89		
$a\,^3E_{2g}$ ($a^1_{1g}e^3_{2g}e^2_{1g}$)	2.58	2.38		
$b\,^3E_{2g}$ ($a^1_{1g}e^3_{2g}e^2_{1g}$)	2.74	2.55		
$^3A_{2g}$ ($a^1_{1g}e^3_{2g}e^2_{1g}$)	2.81	2.55		
$^1A_{1g}$ ($a^2_{1g}e^4_{2g}$)	3.34	2.77	2.83

a result, the low-energy part of the MRCI spectrum displays now a richer structure: with orbitals optimized in the prior CASSCF step just for the $a^1_{1g}e^3_{2g}e^2_{1g}$ and $a^2_{1g}e^2_{2g}e^2_{1g}$ configurations and maximum spin multiplicity, the relative energies of the spin-orbit MRCI states are 0 (two states), 15, 17, 23, 81, 84, 86 and 94 (again as a doublet) meV. In other words, the magnetic anisotropy energy of the Fe^{2+} d^6 ion is reduced from $\Delta^{d^6}_{D_{6h}}=26$ meV in D_{6h} symmetry to $\Delta^{d^6}_{C_s}=15$ meV when the symmetry is broken by creating a vacancy at a NN Li site. Analysis of the spin-orbit wave functions shows that these effects imply admixture(s) of the $a^2_{1g}e^2_{2g}e^2_{1g}$ components of only tenths of 1% to the low-lying $a^1_{1g}e^3_{2g}e^2_{1g}$ states. Obviously, the more complicated structure of the spectrum

in the lower-symmetry case is related to having slightly different degrees of $a_{1g}^1 e_{2g}^3 e_{1g}^2 - a_{1g}^2 e_{2g}^2 e_{1g}^2$ admixture for different spin-orbit eigenvectors. The relaxed Fe-N bond lengths are in both cases, without and with a Li-ion vacancy, 1.88 Å. According to experimental investigations [13, 14], the Li-ion vacancies mainly occur within the Li_2N planes.

Remarkably, our computational results for the magnetic anisotropies of Fe^{1+} d^7 and Fe^{2+} d^6 centers within the solid-state matrix of Li_3N find strong support in recent experimental data on $Li_{3-x-2y}Fe_x^{1+}Fe_y^{2+}N$, that indicate magnetic anisotropy energies $\Delta_{x\to0} = 13$ meV in the very dilute case and $\Delta_{x\gg y} = 27$ meV for high concentration of Fe [16]. These drastic variations in the measurements can be assigned to the presence of a finite amount of Li-ion vacancies. An intrinsic load of vacant Li sites has been indeed found experimentally for Li_3N, in the range of ~1% [22], which suggests that for keeping overall charge neutrality Fe ions in the immediate neighborhood of such vacancies might adopt a Fe^{2+} d^6 configuration. The reason no connection has been made so far between these variations of the magnetic properties and the possible predominance of Fe^{2+} d^6 species in the very dilute case is the fact that the d^6 ground-state configuration is ussually associated for linear coordination with a $d_{z^2}^2 d_{xy}^1 d_{x^2-y^2}^1 d_{yz}^1 d_{zx}^1$ orbital occupation [10–12] for which single-ion anisotropy can only occur through weaker, second-order SOC's. The good agreement between our MRCI value $\Delta_{C_s}^{d^6} = 15$ meV and the experimentally derived $\Delta_{x\to0} = 13$ meV makes therefore plausible the scenario in which the magnetic properties in the dilute regime are mainly determined by Fe^{2+} d^6 $(a_{1g}^1 e_{2g}^3 e_{1g}^2)$ ions with broken-symmetry nearby surroundings. Additional support is provided by the good agreement between the MRCI result $\Delta_{D_{6h}}^{d^7} = 30$ meV (see Table I) and the experimental estimate $\Delta_{x\gg y} = 27$ meV at large concentrations of Fe.

Resonant inelastic x-ray scattering (RIXS) measurements on the Fe:Li_3N system might throw fresh light on the problem. The high resolution achieved nowadays in RIXS should allow to directly verify our prediction of a distinct peak at 0.15–0.20 eV for the Fe^{2+} d^6 electron configuration. According to our computational results, the position of these crystal-field excited states is about the same in D_{6h} symmetry (see Table II) and when the symmetry is broken by creating a Li vacancy next to the Fe^{2+} d^6 center. That post-CASSCF quantum chemistry calculations can describe the RIXS d–d excitation spectra with very good accuracy has been convincingly shown already for TM ions in a variety of environments [23–26]. Another experimental technique capable of verifying the existence of Fe^{2+} d^6 ions in Fe:Li_3N is Mössbauer spectroscopy. In addition to stimulating further experimental investigations, our computational data define the frame for subsequent model-Hamiltonian constructions for addressing the magnetodynamics of this system [27, 28].

Aspects which remain to be clarified is the role of spin-phonon couplings in under-barrier spin relaxation [27] but also the occurence of clustering effects among the Fe-ion substitutes and of sizable magnetic exchange between proximate Fe sites.

To summarize, our *ab initio* data put into the spotlight the linearly coordinated Fe^{2+} d^6 ion as candidate for viable SMM behaviour. The calculated magnetic anisotropy splitting of 26.3 meV (i.e., 305 K) in D_{6h} symmetry compares favorably to values measured (28 meV [7] and 27–37 meV [8, 16]) or computed by similar theoretical methods (26 meV [7]) for Fe^{1+} d^7 species with linear coordination, among the largest so far in the research area of SMM's. This substantial spin-reversal energy barrier of the Fe^{2+} ion is associated with a $a_{1g}^1 e_{2g}^3 e_{1g}^2$ ground-state electron configuration, not anticipated by earlier DFT calculations for TM species in such an environment [10–12] and made possible through a subtle interplay between ligand/crystal-field splittings and on-site Coulomb interactions. The effects we point out here warrant more detailed investigations of both iron(I) and iron(II) complexes with linear or quasilinear two-ligand coordination. For iron(II), engineering of the $^5E_{2g} - {}^5A_{1g}$ splitting towards larger values would allow large magnetic anisotropy barriers also for symmetries much lower than D_{6h}.

Methods

All *ab initio* calculations were carried out with the quantum chemistry package MOLPRO [20], using the room-temperature lattice parameters reported in Ref. [21]. To compute the magnetic anisotropy and the on-site d–d excitation spectrum, an embedded cluster consisting of one central Fe ion, the two NN NLi_6 hexagonal plaquettes and the nearby two Li sites on the z axis was considered. The solid-state surroundings were modeled as a finite array of point charges fitted [29] to reproduce the crystal Madelung field in the cluster region [30]. We applied all-electron Douglas-Kroll basis sets of triple-zeta quality for the central Fe ion [31] and all-electron triple-zeta basis sets for the two NN nitrogen ligands [32] and the Li species, supplemented with polarization functions. For the CASSCF calculations, we employed an active space of five $3d$ orbitals at the Fe site and seven (six) electrons for the Fe^{1+} d^7 (Fe^{2+} d^6) valence configuration; the orbitals were optimized for an average of all high-spin (either $S=3/2$ or $S=2$) states. Only the N $2s, 2p$ and Fe $3s, 3p, 3d$ electrons were correlated in the subsequent MRCI treatment.

---

[1] L. Bogani and W. Wernsdorfer, *Nat. Mater.*, 2008, **7**, 179–186.

[2] R. Sessoli, D. Gatteschi, A. Caneschi and M. A. Novak, *Nature*, 1993, **365**, 141–143.

[3] J. D. Rinehart, M. Fang, W. J. Evans and J. R. Long, *Nat. Chem.*, 2011, **3**, 538–542.

[4] J. D. Rinehart, M. Fang, W. J. Evans and J. R. Long, *J. Am. Chem. Soc.*, 2011, **133**, 14236–14239.

[5] S. K. Gupta, T. Rajeshkumar, G. Rajaraman and R. Murugavel, *Chem. Sci.*, 2016, **7**, 5181–5191.

[6] A. L. Svitova, K. B. Ghiassi, C. Schlesier, K. Junghans, Y. Zhang, M. M. Olmstead, A. L. Balch, L. Dunsch and A. A. Popov, *Nat. Commun.*, 2014, **5**, 3568.

[7] J. M. Zadrozny, D. J. Xiao, M. Atanasov, G. J. Long, F. Grandjean, F. Neese and J. R. Long, *Nat. Chem.*, 2013, **5**, 577–581.

[8] A. Jesche, R. W. McCallumm, S. Thimmaiah, J. L. Jacobs, V. Taufour, A. Kreyssig, R. S. Houk, S. L. Bud'ko and P. C. Canfield, *Nat. Commun.*, 2014, **5**, 3333.

[9] J. Klatyk, W. Schnelle, F. R. Wagner, R. Niewa, P. Novák, R. Kniep, M. Waldeck, V. Ksenofontov and P. Gütlich, *Phys. Rev. Lett.*, 2002, **88**, 207202.

[10] P. Novak and F. R. Wagner, *Phys. Rev. B*, 2002, **66**, 184434.

[11] V. P. Antropov and V. N. Antonov, *Phys. Rev. B*, 2014, **90**, 094406.

[12] L. Ke and M. van Schilfgaarde, *Phys. Rev. B*, 2015, **92**, 014423.

[13] D. H. Gregory, P. M. O'Meara, A. G. Gordon, J. P. Hodges, S. Short and J. D. Jorgensen, *Chem. Mater.*, 2002, **14**, 2063–2070.

[14] A. G. Gordon, R. I. Smith, C. Wilson, Z. Stoeva and D. H. Gregory, *Chem. Commun.*, 2004, **24**, 2812–2813.

[15] D. Muller-Bouvet, J. P. Pereira-Ramos, S. Bach, P. Willmann and A. Michalowicz, *Inorg. Chem.*, 2014, **53**, 6127–6131.

[16] A. Jesche, L. Ke, J. L. Jacobs, B. Harmon, R. S. Houk and P. C. Canfield, *Phys. Rev. B*, 2015, **91**, 180403.

[17] T. Helgaker, P. Jørgensen and J. Olsen, *Molecular Electronic-Structure Theory*, Wiley, Chichester, 2000.

[18] H.-J. Werner and P. J. Knowles, *J. Chem. Phys.*, 1988, **89**, 5803–5814.

[19] A. Berning, M. Schweizer, H.-J. Werner, P. J. Knowles and P. Palmieri, *Mol. Phys.*, 2000, **98**, 1823–1833.

[20] H. J. Werner, P. J. Knowles, G. Knizia, F. R. Manby and M. Schütz, *Wiley Rev: Comp. Mol. Sci.*, 2012, **2**, 242–253.

[21] A. Huq, J. W. Richardson, E. R. Maxey, D. Chandra and W.-M. Chien, *J. Alloys & Compounds*, 2007, **436**, 256–260.

[22] H. Schulz and K. H. Thiemann, *Acta Cryst. A*, 1979, **35**, 309–314.

[23] M. Minola, L. Hozoi, D. Di Castro, R. Felici, M. Moretti Sala, A. Tebano, G. Balestrino, G. Ghiringhelli, J. van den Brink and L. Braicovich, *Phys. Rev. B*, 2013, **87**, 085124.

[24] M. Guo, E. Kallman, L. K. Sørensen, M. G. Delcey, R. V. Pinjari and M. Lundberg, *J. Phys. Chem. A*, 2016, **120**, 5848–5855.

[25] K. Kunnus, W. Zhang, M. G. Delcey, R. V. Pinjari, P. S. Miedema, S. Schreck, W. Quevedo, H. Schröder, A. Föhlisch, K. J. Gaffney, M. Lundberg, M. Odelius and P. Wernet, *J. Phys. Chem. B*, 2016, **120**, 7182–7194.

[26] N. A. Bogdanov, V. Bisogni, R. Kraus, C. Monney, K. Zhou, T. Schmitt, J. Geck, A. O. Mitrushchenkov, H. Stoll, J. van den Brink and L. Hozoi, *J. Phys. Condens. Matter*, 2017, **29**, 035502.

[27] A. Lunghi, F. Totti, R. Sessoli and S. Sanvito, *Nat. Commun.*, 2017, **8**, 14620.

[28] R. Layfield, F. Guo, B. Day, Y. Chen, M. Tong and A. Mansikamäkki, *Angew. Chem. Int. Ed.*, 2017, DOI:10.1002/anie.201705426.

[29] M. Klintenberg, S. Derenzo and M. Weber, *Comput. Phys. Commun.*, 2000, **131**, 120–128.

[30] B. Roos and U. Wahlgren, MADPOT and MADFIT programs (1969).

[31] N. B. Balabanov and K. A. Peterson, *J. Chem. Phys.*, 2005, **123**, 064107.

[32] T. H. Dunning, *J. Chem. Phys.*, 1989, **90**, 1007–1023.